Time-of-flight absorption and scattering spectroscopy of pharmaceutical tablets

Jesper Håkansson and Shazia Farooq,
Lund Univeristy,
Jesper.Max.Olof.Hakansson@gmail.com
Shazia.Enayat@gmail.com

August 23, 2010

Abstract

Near infrared photon time-of-flight spectroscopy is a fast, non-destructive and non-invasive measurement technique that show potential for quality control in the pharmaceutical industry.

The aim of this masters thesis is to use near infrared photon time-of-flight spectroscopy to measure the concentration of a known chemical compound in a pharmaceutical tablet.

The absorption spectra of the active pharmaceutical compound is weak. Therefore to estimate the concentrations, accurate absorption measurements on several wavelengths are needed. The time-of-flight results from a large set of tablets with a wide variety of properties i.e. particle size and concentrations, and known compound concentrations are used in a PLS regression to make a model of the absorption-concentration dependency. From this model the concentration is calculated.

The absorption is measured with 2% precision and this measure the concentration within 15% precision. This is enough to distinguish between the highest and the lowest concentrations in the tablet set. The results are promising and show great potential for improvement.

Contents

Chapter 1

Introduction

In 1666, Sir Isaac Newton discovered that white light could be dispersed into a continuous series of colours. He called this phenomenon a "spectrum". Two centuries later, in 1859 Gustav Kirchhoff established that each element has its own unique spectrum and by studying the spectra of something unknown it is possible to determine its chemical composition and spectroscopy is born as a field of science.

Since then 15 Nobel prizes has been awarded to discoveries in this field and it has been developed into a reliable technique. Today it is used through out industry and research as the technique of choice for a wide variety of measurements.

Conventional spectroscopy becomes more difficult for scattering mediums as the intensity can not directly be used to calculate the absorption. This is mostly solved with frequent and expensive calibrations. Recent developments in near infrared photon time-of-flight spectroscopy enables non-invasive and non-destructive measurements of the absorption separate from the scattering.

The purpose of this thesis is to determine the concentration of active pharmaceutical ingredient in a series of tablets using near infrared photon time-of-flight spectroscopy.

1.1 Outline

Chapter 2: Spectroscopy in turbid media. It is a short explanation about the underlying physics for spectroscopic measurements an turbid media as well as a general description of the most common spectroscopy techniques.

Chapter 3: Experimental setup. It is an explanation of the setup used in our measurements and the function of the individual devices.

Chapter 4: Theory. It is an introduction to the analysis tools used to handle the data from the measurements, including an explanation of the regression used for evaluation of the resulting absorption.

Chapter 5: Results. It is the results of measurements with following analysis and regression.

Chapter 6: Conclusion

Appendix:

1.2 Abbreviations and Notations

API	-Active Pharmaceutical Ingredient	MVLA	-Multivariate Linear Analysis
AOTF	-Acousto Optic Tunable Filter	NIR	-Near Infrared
CFD	-Constant Fraction Discriminator	PCA	-Pricipal Component Analysis
DA	-Diffusion Approximation	PCF	-Photonic Crystal Fiber
EM	-Electromagnetic	PCR	-Pricipal Component Regression
FWHM	-Full Width at Half Maximum	PLS	-Partial Least Squares
IR	-Infrared	PMT	-Photomultiplying Tube
IRF	-Instrument Response Function	PTOF	-Photon Time Of Flight
MC	-Monte Carlo	RTE	-Radiative Transfer Equation
MCA	-Multi-channel Analyzer	SC	-Supercontinuum
MCP	-Micro-chanel Plate	TCSPC	-Time Correlated Single Photon Counting

$\hat{b}$	-Regression coefficient	μ_t	-Extinction coefficient
$\chi^2(\mathbf{p})$	-Chi-squared error	n	-Refractive index
D	-Diffusion coefficient	P	-Loading matrix
E	-Residual	$\mathbf{p}$	-Curve parameters
$\varepsilon(\mathbf{r}, t, \hat{s})$	-Source	$p(\hat{s}, \hat{s}')$	-Scattering probability
$\mathbf{h}$	-Step size, curve fitting	$R(\theta_i)$	-Fresnel reflectivity
$I(L)$	-Intensity at a position	$\mathbf{T}$	-Score matrix
I_0	-Initial intensity	$T(\rho, t)$	-Fresnel transmitivity
$I(\mathbf{r}, t, \hat{s})$	-Specific intensity	U_d	-Diffuse intensity
$\mathbf{J}$	-Jacobian	v	-Speed of light in medium
L	-Path length	$\mathbf{W}$	-Weights matrix
λ	-Wavelength	X	-Independent variable
m	-Number of atoms in a molecule	Y	-Dependent variable
μ_a	-Absorption coefficient	$y(t_i)$	-Measured curve
μ_s	-Scattering coefficient	$\hat{y}(t_i; \mathbf{p})$	-Simulated curve

Chapter 2

Spectroscopy in turbid media

To make this thesis more accessible to everyone we begin with a brief explanation of the underlying physics of these experiments and near infrared spectroscopy. The chapter ends with a few techniques to do spectroscopy in highly scattering or, as it is called in this context, turbid media.

2.1 Interaction of light in turbid media

Electromagnetic radiation ranges from cosmic rays to microwave region. The only differences is their wavelengths. When EM radiation interacts with matter the fundamental processes of scattering i.e. excitation and re-radiation, and absorption i.e. transforming part of radiation into other form of energy e.g. heat energy, takes place. These are the processes that make the sky blue, sugar white and blood red.

2.1.1 Reflection

When light falls at the boundary between two media of different refractive index the light which is reflected back is called specular reflection. The reflected intensity and direction is dependant on the incident angle, θ_i, polarization of light[1], shape and structure of the surface. If the polarization is neglected, reflection is given by, $\theta_i = \theta_r$, and angle of refraction is given by Snell's Law,

[1] Transverse waves such as light have a polarization, a plane in which the wave oscillates. Polarized light is light were the photons all have the same polarization

$$n_i \sin(\theta_i) = n_r \sin(\theta_t) \tag{2.1}$$

The amount of light reflected at the surface for p- and s-polarised light is given by Fresnel's Law,

$$R_p = \left(\frac{n_1 \cos\theta_t - n_2 \cos\theta_i}{n_1 \cos\theta_t + n_2 \cos\theta_i} \right)^2 \tag{2.2}$$

$$R_s = \left(\frac{n_1 \cos\theta_i - n_2 \cos\theta_t}{n_1 \cos\theta_i + n_2 \cos\theta_t} \right)^2 \tag{2.3}$$

In our case the laser beam is incident perpendicular to tablet surface, i.e. $\theta_i = 0$. Since the refractive index of our pharmaceutical tablets are about 1.5, approximately 4% of light is reflected back at the air-tablet boundary. Total internal reflection takes place where critical angle $\theta_c \approx 42^\circ$, light with greater angle of incidence will then be totally reflected at the boundary.

2.1.2 Scattering

There are two kinds of scattering. Elastic scattering when there is no change in photon energy e.g. Rayleigh and Mie scattering and inelastic scattering when there is a change in photon energy e.g. Raman scattering.

The Rayleigh approximation is valid when particle size is much smaller than the incident wavelength, whereas for all other homogeneous and spherical particles of a size comparable to incident wavelength, Mie scattering is valid. The scattering dependence of wavelength varies with particle size from λ^{-4} for smaller to λ^{-2} for larger particles. Raman scattering is normally an improbable process where part of the photon energy is transferred to or from a molecule[3].

The probability for a photon to get scattered in a medium is described by the scattering coefficient, μ_s, which is the mean amount of scattering events per unit length. It's inverse gives scattering mean free path which gives the average distance a photon travel between each scattering event.

2.1.3 Absorption

If a photon's energy is equivalent to the difference in energy between the electronic states of an atom, the photon can get absorbed and the atom

exited. Since the absorption spectra of an atom is unique, it can be used for identification. Absorption is modelled by Beer-Lambert's Law,

$$I(L) = I_0 \exp(-\mu_a L) \tag{2.4}$$

where I_0 is initial photon intensity, I is transmitted intensity, L is path length and μ_a is absorption coefficient which gives the probability of a photon to get absorbed in a medium per unit of propagation length. The inverse gives absorption mean free path length which defines an average distance a photon travel before getting absorbed[2].

2.2 Near Infrared Spectroscopy

The near infrared, NIR, region lies between 780nm to 2500nm, beginning in the visible red region and continuing till the mid IR region. These energies correspond to the energies of molecular vibration and rotation and it is often used to identify organic molecules.

2.2.1 Molecular Vibrations

An atom has three degrees of freedom, so for molecules consisting of m atoms there will be $3m$ degrees of freedom. In the case of non linear molecules, 3 of these degrees of freedom correspond to the rotational and 3 to the translational motion of the molecule, so the molecule has $3n - 6$ fundamental vibrational modes whereas in the case of linear molecules 2 degrees of freedom correspond to rotational and 3 to translational motion of molecule, and left linear molecules with $3m - 5$ degree of fundamental vibrational modes. Fundamental vibrations are also called normal modes of vibration[4].

The number of bands calculated do not always corresponds to the observed. Additional bands can occur due to overtones, difference and combination of fundamental frequencies and Fermi resonance. Fermi Resonance occurs when two different modes, mostly normal and overtone, have the same energy. When they interact with each other they exchange energies and resonates. This causes a shift in energies and intensities of the band. An example of band degeneracy is carbon dioxide, CO_2, which is linear and has four fundamental vibrational modes, see Fig. 2.1.

The two bending vibrations in Fig. 2.1b and 2.1d are similar except their direction, therefore they are degenerate. The symmetrical stretch is IR inactive as it does not produce any change in the molecule's dipole moment. Carbon dioxide is an example where the number of absorption bands are less than actual vibrational modes as only two out of four IR modes can be

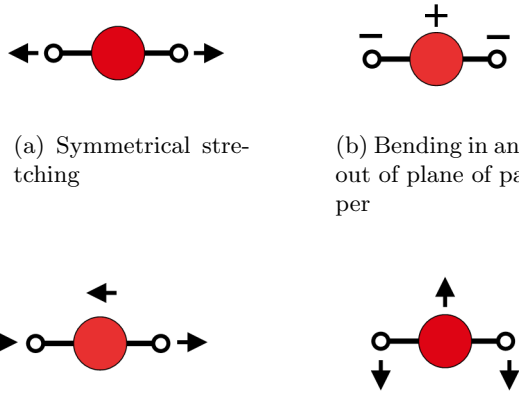

(a) Symmetrical stretching

(b) Bending in and out of plane of paper

(c) Asymmetrical stretching

(d) Bending in the plane of paper

Figure 2.1: Fundamental vibrational modes of CO_2 and its symmetry.

observed. Bending vibrations occurs at lower frequencies corresponding to stretching vibrations.

2.2.2 NIR Spectroscopy in pharmaceutical applications

NIR spectroscopy is a widely used measurement technique to identify elements in a sample both qualitatively and quantitatively. One of the major areas covered by NIR spectroscopy is pharmaceutical science[5] [3]. Spectroscopic measurements on pharmaceuticals are frequently difficult as the samples are highly scattering which affects the measured absorption for most spectroscopy techniques. The NIR region with its longer wavelength have less scattering and because of this it is often a sensible choice.

The advantage of this technique is that it is faster, nondestructive and need no sample preparation. The method is used for identifying raw materials, quality control, particle sizing, concentration determination and process monitoring of pharmaceutical ingredients[6][7].

The overtone and combination bands observed, in the NIR, are quite broad leading to a complex spectra. Since the NIR region is dominated by vibrational and rotational modes, the absorption is small. NIR requires statistical methods e.g. multivariate calibration, to model sample's NIR spectral response and extract the desired chemical or physical properties. This method is also used to distinguish between different crystalline forms of materials, because the effectiveness of drugs does not only depends upon its

chemical formula but also on the granulate physical structure e.g. particle size and shape. For quantitative measurement of components in tablets transmission is preferred over reflectance spectroscopy because the light have a longer pathlength in the sample giving a stronger signal. However for turbid media e.g. powders, the transmitted intensity is to weak [8]. The structural properties of a tablet affect scattering which in turn change the optical pathlength in the tablet[9].

2.3 Experimental Techniques To Measure Optical Parameters in turbid media

There are a number of techniques that can be use in-vivo and in-vitro to determine the scattering and absorption coefficients in a turbid medium.

2.3.1 Spatially Resolved Spectroscopy

For spatially resolved spectroscopy the intensity is measured at a number of different distances to a point source. The optical properties can then be derived from these intensity to distance relations. The light source used in this case is can both be continuous and pulsed but then the pulse length must be much larger than the photon propagation time i.e. nanoseconds. The technique is quite cheap and simple, but sensitive to inhomogeneities in the sample and it only works for small source detector separation. For greater volumes it is only possible to measure the effective attenuation.

2.3.2 Time Domain Spectroscopy

Time domain spectroscopy is also known as time-of flight spectroscopy, TOFS. In this technique the temporal pulse shape of a transmitted or reflected picosecond pulse from a point light source is repeatedly measured. As scattering delays the pulse while absorption increase with longer pathlength the pulseshape can be used to calculate these optical properties. The main advantage of this method is that both μ_s' and μ_a can be separated but at the cost of a worse signal-to-noise ratio.

2.3.3 Frequency Domain Spectroscopy

Instead of using a pulsed source a sinusoidal modulated source can be used. The photon flux detected by the detector is then also sinusoidal but at-

tenuated and with a phase shift. Depending on the scattering properties the oscillations will be delayed relative to source as it passes through the medium. When the scattering is known the absorption can be calculated from the attenuation. Technically this method is quite simple as it works in range of 100 MHz and get better signal-to-noise ratio, but does not provide as much information compared to time-of flight spectroscopy. Better results can be obtained if several different modulation frequencies are used for evaluation.

Chapter 3

Experimental Setup

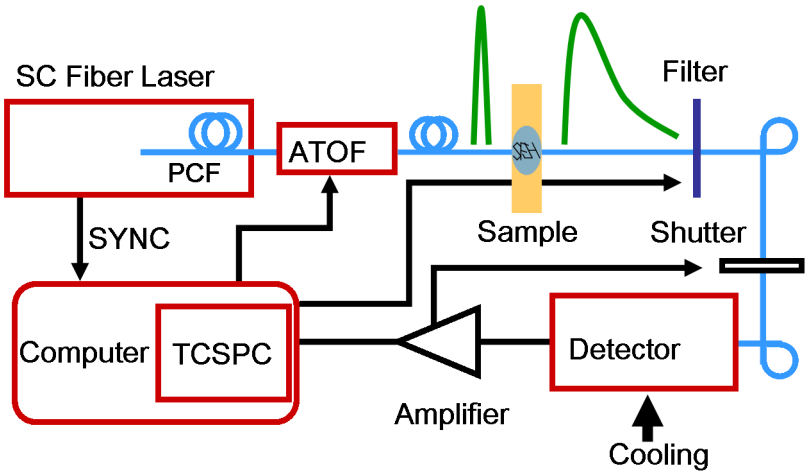

Figure 3.1: The schematics for the NIR PTOF setup to measure the absorption and scattering spectra.

A measurement begin with that a short picosecond pulse and a SYNC signal is generated in the fiber laser. The pulse is then spectrally broadened into a supercontinuum when it pass through the PCF. The AOTF selects a narrow wavelength span which is transmitted to the sample. The pulse is temporally broadened by the sample. After the filter attenuates the pulse until only one photon is transmitted, the photon is registered at the detector. The detector signals the TCSPC card which starts an internal clock. The SYNC signal arrives and stop the clock. The measurement is repeated until a histogram of the measured time forms the pulse shape.

3.1 Experimental procedure

The detector need to be cooled down to -80°C before starting the measurements. Fill the cooling dewar with liquid nitrogen. Place the pump system into the dewar and let it cool down. It is important that the dewar is leaking at this point so that no pressure is built up. If the dewar is sealed, the temperature goes down below -80°C in a few minutes. Turn on the laser to full power.

When the dewar and pump system is cooled down and the temperature in the dewar is stable, close the dewar. Set the pressurised nitrogen to 0.3 atm., and start the temperature control system. Wait for the PMT to slowly cool down to -80°C. If the exhaust starts to contain liquid nitrogen, the pressure in the dewar is to high and needs to be released.

When the PMT has finished cooling down and the temperature has stabilised, set the voltage over the PMT to 3000 V. Start the computer programs that control the TCSPC card, ATOF and filter.

Select the desired wavelength in the ATOF program, place the sample in the sample holder, set the fibers so that they connect with the surface of the sample and set the filter to high attenuation. Open the shutter and set the filter so a 100kHz signal is measured. Measure the pulseshape. Close the shutter and switch the sample with the IRF. Set the filter so 100kHz signal is measured and measure the pulseshape. All the seven wavelengths; 1100nm, 1150nm, 1180nm, 1210nm, 1240nm, 1275nm and 1300nm are consecutively measured for the tablet, each for 80 cycles á 0.25s after which the measurement is repeated for the IRF.

Load the measurements in to the analysis software, find the peaks, sum the cycles in four groups and fit the result with the model.

3.2 Supercontinuum Fiber Laser

The light source used is Fianum SC-500-6, a pulsed laser with the wide range of 500-1850 nm. This is a ytterbium fiber laser operating at 1066nm and 80 MHz. A broad spectrum called a supercontinuum, SC, is then generated in the photonic chrystal fiber, PCF, by spectrally broadening the laser pulse through 4-wave mixing and stimulated Raman scattering.

The width of the spectrum is very dependent on the laser power because of the reliance on nonlinear effects. When the power is decrease the edges of the generated spectrum are the first to disappear. Another important

factor is the relative detuning between the wavelength of the pumping laser and the zero dispersion wavelength of the PCF. This affects not only the shape of the spectrum but also which physical mechanisms governs the SC generation.

3.3 GRIN Fibers

To transport light to and from sample in the setup GRIN fibers of 600 μm diameter called G600/840N from A.R.T. Photonics are used. The reason for using GRIN fiber over other types of fiber is to avoid temporal broadening of the pulse due to multimodal dispersion. This is when part of the light takes a longer way through the fiber compared to the other part.

3.4 Acousto-Optic Filter

The purpose of the acousto-optic tunable filter, AOTF, is to transmit only the desired part of the SC. The AOTF used is from Crystal Technology and work in a span between 900 - 1550 nm. The obtained pulses are typically shorter than 50 ps full width at half maximum, FWHM, and have less than 8 nm FWHM.

An AOTF is a device that transmit only a selected part of a much broader spectrum. The acousto optic effect is when stress and strain from vibrations alters the refractive index of an optical medium. In an AOTF a optical medium is made to vibrate by alternating electric voltage over a piezoelectric crystal. The periodic refractive index cased by the vibrations makes a grating, scattering the incoming light. By choosing the correct vibration frequency, light of the desired wavelength is focused on a spot where it is collected and transmitted.

3.5 Detector

The NIR spectral range is between 900-1400 nm for which a InP/InGaAsP detector is suitable. The detector we use is a R3809U-68 from Hamamatsu Photonics covering the whole of the desired span. To be able to count single photons the detector is equipped with a MCP-PMT and cooled down to -80°C. Cooling not only reduce the thermal noise but also enhance the spectral range and sensitivity of the detector. The output signal from the detector is amplified by HFAC-26, Becker & Hickl, amplifier, which also

controls a shutter that protects the detector from overloading.

3.6 Detector cooling

The cooling system used is a R3809U-50/1406 from Research Inc. It uses liquid nitrogen pumped from a dewar to cool the detector. The pumping is automatically controlled using pressurised nitrogen. To make the pumping more reliable and efficient the pressure loss from the dewar was controlled with an aluminium ring we made. This caused the temperature to go down faster but much of the dampening was lost causing the temperature to oscillate.

3.7 TCSPC Technique

To measure the time delay we use SPC-300, TCSPC card from Becker & Hickl. The TCSPC method works on measuring the time delay between two events e.g. between a photon arriving at a detector and a reference signal. By repeating the same measurement several times a statistical distribution of time delay is achieved. This method is also use for measuring excited state life time of free atom and fluorescence life time.

To avoid fluctuation in amplitude in signal from detector a constant fraction discriminator, CFD, is used. It improves timing by compensating for variation in amplitude and creates threshold for noise by rejecting pulses with high and low amplitudes.

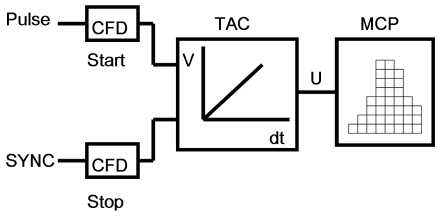

Figure 3.2: A graphical representation of the TCSPC card function.

This pulse is then sent to the time-to-amplitude converter, TAC, which starts an internal clock on the arrival signal pulse. The clock stops when a reference pulse, SYNC, from the light source is detected at the TAC. The output from the TAC is an electric pulse with an amplitude proportional to time delay between the two input pulses. This voltage is send to multi-channel analyzer, MCA, that converts the analog signal to a digital. For each corresponding voltage MCA adds one count to the corresponding channel. By repeating this procedure several times a

statistical histogram is created by MCA for the time difference SYNC and detected photon.

To avoid pile up error due to multiple photon detection, probability of detecting one photon per laser pulse should be kept below 1%. The loss in intensity can be minimized by using a laser source with high repetition rate e.g.50-100 MHz. This is normally not a problem as the detector will get overloaded before the limit is reached [13].

Temporal resolution in TCSPC method is limited by detector transit time spread of single photon pulse and electronic systems triggering accuracy, resulting in impulse response in order of 10-100ps.

The technique is based on detection of a single photon and is very sensitive as it can be used even when detected signal is weak with good resolution which is an advantage.

3.8 IRF measurements

The instrument response function, IRF, is a function that describes how a measurement is affected by the setup. Ideally this is a measurement without a sample but where the pertubations caused by the setup are the same as in a measurement with a sample. This is a bit more complicated in a PTOF as which modes are filled in the fibres are dependant on the scattering of the sample. To solve this problem the IRF is measured on an object which cause very small temporal broadening but manages to fill the same modes as a sample.

We measure the IRF using a folded piece of paper which have been several times printed black. Paper is good because it cause a very small temporal broadening but scatter enough to mimic the sample.`[quote stefan paper on paper]`

3.9 Tablets set

The tablets measured on was Seloken tablets which is beta blocker used to treat various cardiovascular diseases such as high blood pressure.The active ingredient is Metoprolol.

The tablets of the 'API set' were made at Astra Zeneca Mölndal in February. The tablet granulate was weighed on a scale within a percent of 500 mg after which it was placed in a container that it self was placed in a

Granulate	1	5	11	13	17	19
Metoprolol	180	190	200	210	220	220
Metoprolol batch	A	A	B	A	A	B
MCC	255.48	247.76	240	232.24	224.52	224.52
Laktos	74.52	72.24	70	67.76	65.48	65.48
K90	14	14	14	14	14	14
Collod. Silica.	18	18	18	18	18	18
Sodium starch	80	80	80	80	80	80
Mg stearat	7.6	7.6	7.6	7.6	7.6	7.6

Table 3.1: The chemical contents of the different granulates. Granulate 17 and 19 are chemically identical but the Metoprolol is made in a different patch.

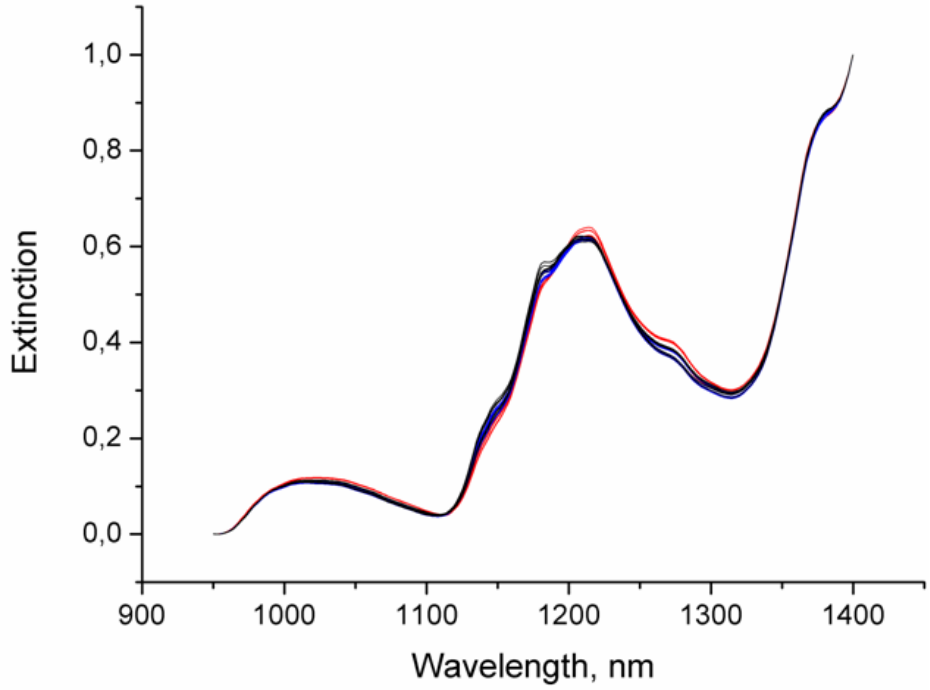

Figure 3.3: The extinction spectrum of the 'API set' as measured in Astra Zeneca. The sifts are differentiated by colour.

machine which pressed the tablet. The pressure used was controlled using a button which the longer it was pressed the more pressure was applied. As the pressure rose very quickly it was difficult to control the exact pressure. We estimate the tablets to be made with 2 ± 0.25t pressure.

The 'API set' consists of a total of 54 tablets. The were made of 6 different granulates: 1, 5, 11, 13, 17 and 19 each divided into three sift size categories: below 150μm, 150μm-450μm and above 450μm with 3 duplicates of each combination. The major compounds of the granulate can be seen in Tab.3.1

Another set of 10 tablets of nonsifted granulate 11 with different pressure were made in June.
Maybe a graph of Thickness and Weight distributions.
Ask AZ what we can publish.

Chapter 4

Theory

As time-of-flight measurements only indirectly measure the optical properties of the sample a good model is needed for the conversion from time-of-flight distribution to absorption and scattering. The two diffusion models we have used during our work with this thesis are a Diffusion Approximation, DA, of the radiative transfer equation and Monte Carlo simulation. The absorption and scattering is then calculated by curve fitting a model to the measurements. Then we use regression on the data to calculate the API concentration.

4.1 Modelling

4.1.1 Diffusion Approximation

A common model to describe the migration of photons in turbid media is the diffusion approximation of the radiative transfer equation, RTE. The time dependent RTE for photon migration is,

$$\begin{aligned}\frac{1}{v}\frac{\partial}{\partial t}I(\mathbf{r},t,\hat{s}) + \hat{s}\cdot\nabla I(\mathbf{r},t,\hat{s}) &= -\mu_t I(\mathbf{r},t,\hat{s}) \\ &+\frac{\mu_t}{4\pi}\int_{4\pi} p(\hat{s},\hat{s}')I(\mathbf{r},t,\hat{s})d\omega' + \varepsilon(\mathbf{r},t,\hat{s})\end{aligned} \tag{4.1}$$

where $I(\mathbf{r},t,\hat{s})$ the specific intensity at a time, t, a place, $\mathbf{r}$, in the direction $\hat{s}$, v is the speed of light in the medium, $\mu_t = \mu_s + \mu_a$ is the extinction coefficient, $\varepsilon(\mathbf{r},t,\hat{s})$ is the source term and $p(\hat{s},\hat{s}')$ is the scattering function

that defines the probability for a photon moving in direction $\hat{s}$ to be scattered into direction $\hat{s}'$.
If the following simplifying assumptions are made,

1. the specific intensity is assumed to be almost isotropic,
2. the scattering function $p(\hat{s}, \hat{s}')$ is assumed to depend only on the scalar product $\hat{s} \cdot \hat{s}'$,
3. and the time variation of the diffuse flux vector over a length of $1/\mu_s'$ is assumed to be negligible with respect to the vector itself.

Solution in uniform media

The formula for diffuse intensity is then,

$$U_d(\mathbf{r}, t) = \frac{v \exp\left(-\frac{|\mathbf{r} - \mathbf{r}'|^2}{4Dvt} - \mu_a vt\right)}{4\pi(4\pi Dvt)^{3/2}} \tag{4.2}$$

where $D = 1/3\mu_s'$ is the diffusion coefficient, μ_s' is the scattering coefficient when compensating for the angle dependence of scattering in the medium and $\mathbf{r}'$ is the position of the source.

Approximate solution in slab

To model the photons that leave the medium alternating negative and positive sources are mirrored at the boundaries reducing the intensity at the edges to zero.

Because of the refractive index difference at the boundary some of the photons are going to be reflected, this is modelled by extrapolating the boundary by a distance z_e,

$$z_e = 2AD \tag{4.3}$$

were A is,

$$A = \frac{1 + 3\int_0^{2/\pi} R(\theta_i)\cos^2(\theta_i)\sin(\theta_i)d\theta_i}{1 - 2\int_0^{2/\pi} R(\theta_i)\cos(\theta_i)\sin(\theta_i)d\theta_i} \tag{4.4}$$

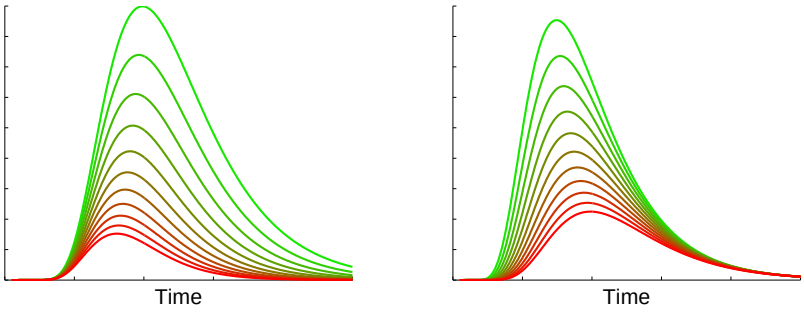

(a) Absorption (b) Scattering

Figure 4.1: This is the curves generated by the DA model. In Fig. 4.1a μ_a increase as the curves go red. In Fig. 4.1b μ_s increase as the curves go red.

and where $R(\theta_i)$ is the Fresnel reflectivity. The resulting equation for the transmittive case is then,

$$\begin{aligned} T(\rho,t) =& \frac{\exp\left(-\mu_a v t - \frac{\rho^2}{4Dvt}\right)}{2(4\pi Dv)^{3/2}t^{5/2}} \\ & \cdot \sum_{m=-\infty}^{+\infty}\left[z_{1,m}\exp(-\frac{z_{1,m}^2}{4Dvt}) - z_{2,m}\exp(-\frac{z_{2,m}^2}{4Dvt})\right] \end{aligned} \tag{4.5}$$

This is the equation we have used to model the time-of-flight distribution for our measurements.

Discussion of applicability to a tablet

The effect of different scattering and absorption can be seen in Fig. 4.1. When the absorption increase the later parts of the curve is attenuated more than the early this makes the pulse peak earlier. The scattering is what broadens the pulse by delaying photons, therefore the pulse peak arrive later when the scattering is high.

To reduce the impact of noise in the measurements only the parts of the curve with a high count rate are used i.e. between where the curve reach 80% of maximum and where it goes down to 20% on the other side of the maximum.

The DA model is also lacking in that it models a point source and a point detector. As the width of the fibers we use are 1/5th of the tablet thickness

this is a cause for concern. Another part that need to be investigated is the reflected and transmitted light at the edge of the tablet. The top and bottom boundaries are modelled but, as the DA use a semiinfinite medium, the sides are ignored. Both of these two problems are explored in greater detail in Results, Sec. 5.2.

4.1.2 Monte Carlo

Another method to simulate the time resolved distribution is to use the Monte Carlo method. It is a group of algorithms that is based on repeated random sampling to compute the results. Using the RTE to repeatedly simulate individual photon movements gives very accurate results but it is also a very time consuming procedure.

4.1.3 The inverse problem

The above mentioned models can not be used to directly calculate the absorption and scattering from the temporal distribution. This is solved with a curve fitting algorithms that iteratively simulate a curve and from a comparison with the measured curve estimate better parameters. These parameters are then simulated and so on.

A problem is that the effect that a different scattering and absorption have on the time distribution curve are similar, see Fig. 4.1. This cause a poorly estimated scattering to result in an equally poorly estimated absorption and vice versa.

4.2 Curve fitting

When minimizing the difference between the the measured curve, $y(t_i)$, and the simulated curve, $\hat{y}(t_i; \mathbf{p})$, of the parameters, $\mathbf{p}$, we use mean squared error as an indicator of how good a fit it is. It is common to include a weight, w_i, into the indicator. It is used to prioritize the parts of the curve which are important and reliable for a good fit. This is called the chi-squared error criterion,

$$\begin{aligned}\chi^2(\mathbf{p}) &= \frac{1}{2}\sum_{i=1}^{m}\left[\frac{y(t_i)-\hat{y}(t_i;\mathbf{p})}{w_i}\right]^2 \\ &= \frac{1}{2}(\mathbf{y}-\hat{\mathbf{y}}(\mathbf{p}))^T\mathbf{W}(\mathbf{y}-\hat{\mathbf{y}}(\mathbf{p})) \\ &= \frac{1}{2}\mathbf{y}^T\mathbf{W}\mathbf{y} - \mathbf{y}^T\mathbf{W}\hat{\mathbf{y}} + \frac{1}{2}\hat{\mathbf{y}}^T\mathbf{W}\hat{\mathbf{y}}\end{aligned} \tag{4.6}$$

To simplify things for us $\mathbf{W}$ is chosen to be the identity matrix. Instead of weights we do not use the parts of the curve more susceptible noise, as explained earlier.

The curve-fitting method used is the Levenberg Marquardt method. It is an iterative method where the parameters are updated with a perturbation $\mathbf{h}$. The permutation is accepted if χ^2 is sufficiently reduced otherwise $\mathbf{h}$ is recalculated. This is repeated until a convergence criteria is fulfilled or the number of iterations exceed a predefined limit.

The Levenberg Marquardt method is a combination of two minimization methods: the gradient descent method and the Gauss-Newton method. They are briefly explained to here make sense of the Levenberg Marquardt method.

4.2.1 The Gradient Descent Method

In the gradient decent method the error is reduced by updating the parameters in the direction of the greatest descent in regard to the squared error criterion. The step size is dependant on the absolute value of the gradient.

The gradient of the chi-squared error function is,

$$\begin{aligned}\frac{\partial}{\partial\mathbf{p}}\chi^2 &= (\mathbf{y}-\hat{\mathbf{y}}(\mathbf{p}))^T\mathbf{W}\frac{\partial}{\partial\mathbf{p}}(\mathbf{y}-\hat{\mathbf{y}}(\mathbf{p})) \\ &= -(\mathbf{y}-\hat{\mathbf{y}}(\mathbf{p}))^T\mathbf{W}\left[\frac{\partial\hat{\mathbf{y}}(\mathbf{p})}{\partial\mathbf{p}}\right] \\ &= -(\mathbf{y}-\hat{\mathbf{y}})^T\mathbf{W}\mathbf{J}\end{aligned} \tag{4.7}$$

where the Jacobian, $\left[\frac{\partial\hat{\mathbf{y}}(\mathbf{p})}{\partial\mathbf{p}}\right]$, is replaced by J for simplicity. The step size is then

$$\mathbf{h}_{gd} = \alpha\mathbf{J}^T\mathbf{W}(\mathbf{y}-\hat{\mathbf{y}}) \tag{4.8}$$

where α is a scalar.

4.2.2 The Gauss Newton Method

The Gauss Newton method reduces the error by assuming that the function is approximately quadratic in the parameters near the optimal solution.

The function is locally approximated with a first-order Taylor expansion.

$$\hat{\mathbf{y}}(\mathbf{p} + \mathbf{h}) \approx \hat{\mathbf{y}}(\mathbf{p}) + \left[\frac{\partial \hat{\mathbf{y}}}{\partial \mathbf{p}}\right] \mathbf{h} = \hat{\mathbf{y}} + \mathbf{J}\mathbf{h} \tag{4.9}$$

Substituting the approximation for the perturbed function in eq. 4.6,

$$\begin{aligned} \chi^2(\mathbf{p}+\mathbf{h}) \approx \frac{1}{2}\mathbf{y}^T\mathbf{W}\mathbf{y} + \frac{1}{2}\hat{\mathbf{y}}^T\mathbf{W}\hat{\mathbf{y}} - \frac{1}{2}\mathbf{y}^T\mathbf{W}\hat{\mathbf{y}} \\ -(\mathbf{y} - \hat{\mathbf{y}}(\mathbf{p}))^T\mathbf{W}\mathbf{J}\mathbf{h} + \frac{1}{2}\mathbf{h}^T\mathbf{J}^T\mathbf{W}\ \mathbf{J}\ \mathbf{h} \end{aligned} \tag{4.10}$$

The perturbation $\mathbf{h}$ that minimizes χ^2 is calculated from, $\dfrac{\partial}{\partial \mathbf{h}}\chi^2 = 0$.

$$\frac{\partial}{\partial \mathbf{h}}\chi^2(\mathbf{p} + \mathbf{h}) \approx -(\mathbf{y} - \hat{\mathbf{y}})^T\mathbf{W}\ \mathbf{J} + \mathbf{h}^T\mathbf{J}^T\mathbf{W}\ \mathbf{J} \tag{4.11}$$

the Gauss-Newton perturbation is then,

$$\left[\mathbf{J}^T\mathbf{W}\mathbf{J}\right] \mathbf{h}_{gn} = \mathbf{J}^T\mathbf{W}(\mathbf{y} - \hat{\mathbf{y}}) \tag{4.12}$$

4.2.3 The Levenberg Marquardt Method

Combining the Gradient Descent and Gauss Newton method into the Levenberg Marquardt method gives,

$$\left[\mathbf{J}^T\mathbf{W}\mathbf{J} + \lambda\mathbf{I}\right] \mathbf{h}_{lm} = \mathbf{J}^T\mathbf{W}(\mathbf{y} - \hat{\mathbf{y}}) \tag{4.13}$$

where a scalar, λ, is used to move the weight between the Gradient Descent and Gauss-Newton method.

When the function is far from the minimum λ is large, the gradient descent method dominates the function and provide a steady convergence. As the function approaches the minimum λ is decreased so that the Levenberg Marquardt method approaches the Gauss-Newton method which typically converges more quickly towards the minimum.

4.3 Multivariate analysis technique

Multivariate analysis is a statistical approach to make data evaluation. These analyses are mainly based on projection techniques. The most common multivariate analysis methods are principle component analysis, PCA, principle component regression, PCR , multivariate linear analysis, MVLA and partial least square, PLS.

4.3.1 Multivariate linear regression

Multivariate linear regression is quite common in spectroscopy when intensities at certain wavelengths are used to predict chemical concentrations.

$$Y = Xb + E \tag{4.14}$$

Where Y is a matrix of dependent variables, X is a matrix of independent variables, E is the residual and $\hat{b}$ is the regression coefficients, defined as

$$\hat{b} = (X^T X)^{-1} X^T Y \tag{4.15}$$

MVLR is one of the simplest method to predict new sample but can only be applicable where few variables (intensities at given variable) are to be extracted. Method fails where collinear data exist.

4.3.2 Principle component analysis

PCA compress data by reducing the dimensionality of data and extract new meaningful variables knows as principle components, PC's. The method describes X by considering useful variation in data and discarding noise. The first PC is chosen in the direction of maximal variation in the data. The remaining residual matrix is then used as input to calculate the next PC. So the second PC is chosen in the direction where the next maximal variation is orthogonal to PC 1 and so on, until the residual become so small it can be considered as noise and thus neglected. The equation for X is given by

$$X = \mathbf{T}P^T + E \tag{4.16}$$

Where P, the loading matrix, represents the principle components in

the original space and **T**, the score matrix, gives the coordinates of all the samples in the new component space.

PCR is a combination of both PCA and MVLA. First PCA is used on the given data, the resultant **T** matrix from eq. 4.16 is used for MVLA. In this method collinear data solving is not a problem but the disadvantage of PCA and PCR method is that the selection of PC's is only dependent on variation in X that might not be optimal for explaining Y.

4.3.3 Partial Least Square

PLS is a powerful multivariate method often used for chemometrics. It is an extension of PCA that finds the components in X correlated to Y which minimize the nonrelevant effect of X[12].

X and Y are correlated through a series of recursive algorithms to generate the PLS components. The first PLS component is in the dimension of X that best correlates with Y. The residual is then used to calculate the next component, like when calculating PCA components.

Chapter 5

Results and Discussion

The aim of this thesis is to determine the Metoprolol content of the tablets. In this chapter we present our results and how they were analysed. We explain how the wavelengths used in the measurements were selected and investigate the measurement procedure.

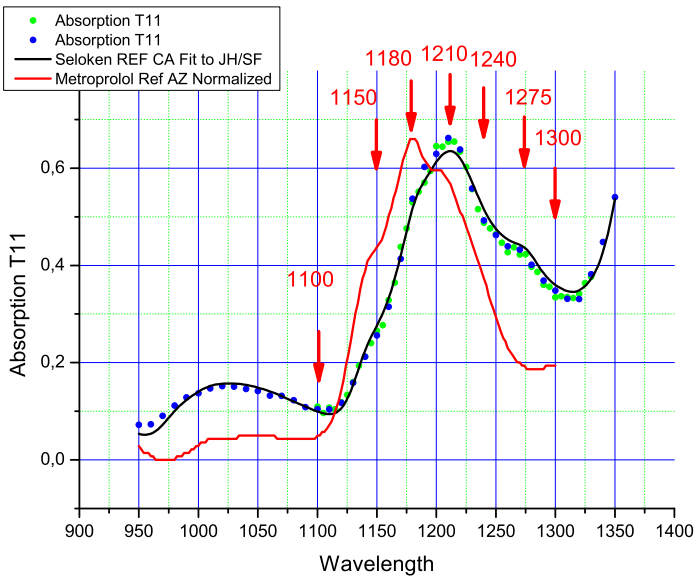

Figure 5.1: The reference spectrum's of Metoprolol and Seloken from Aztra Zeneca and The Seloken spectra measured twice by us on granulate 11. The arrows show the selected wavelengths.

5.1 Wavelength selection

The Seloken and Metoprolol spectra can be seen in Fig.5.1. As the Metoprolol absorption spectra is much weaker than the Seloken spectra we have normalised it to visualize it. The wavelength marked in the graph are the ones measured on. To optimise the estimation of the Metoprolol content in the tablet it is important to find the maximum variation between the two spectra's. It is also important to take the bandwidth of the measurement wavelengths into account as the part with the lower absorption will dominate the measurement and details of the spectra evened out [14]. Another thing to take into account is that the measurement precision decrease when absorption is too low.

Taking these factors into account we chose to use 1210 nm and 1180 nm which is the maximum of the two spectra's. 1275 nm were chosen as it is a minimum in the Metoprolol but not in Seloken spectra while also being reasonably flat. 1100 nm and 1300 nm are minimums for Seloken and 1150 nm and 1240 nm were chosen to sample the spectra equally.

5.2 Measurement

In order to reduce the noise as much as possible and produce precise measurements it is good to measure at as high intensity as possible. Because of the photon pileup where only the earliest of the photons measured during one pulse is recorded there is a theoretical limit where the attenuation is so strong a photon should only be measured in 1% of the pulses. This so that the measured distribution is not distorted by missing the late photons that is hiding behind early ones. It is also good to measure during as short time as possible both because of drift in the measurements and because too long measurement time mean too long work hours.

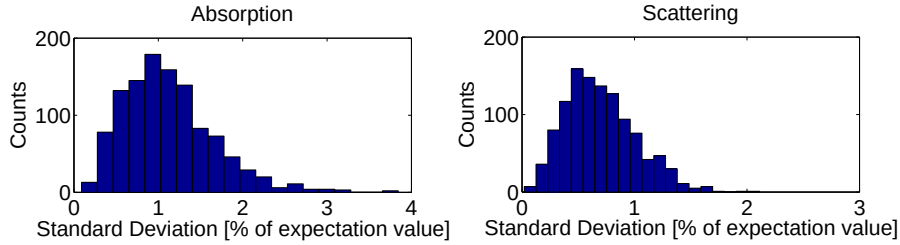

(a) Absorption (b) Scattering

Figure 5.2: The standard deviation of the 'four measurement' scattering and absorption.

How to analyse the measurements

We measured each wavelength four times over 5s at 100kHz for both tablet and IRF measurements. This is a photon measured in 0.13% of the pulses. The mean of these four measurements was then taken as a result. Another way to evaluate the data would be to sum the measured curves and then analyse it. A comparison between the two ways of evaluating the data show there is only a small change. As seen in Fig.5.3 the change in absorption is below 0.3% which is one order less than the standard deviation of a 'four measurement'. Because of the small difference the methods are interchangeable for this setup. Interesting to note is that the variation seems to be dependant on the absorption of the different wavelengths.

Measurement variance

Evaluating as a 'four measurement' gives the benefit of allowing the standard deviation to be calculated from the results as a measure of precision. The resulting histogram can be seen in fig. 5.2. When analysing the different wavelengths, 1100 nm stands out as having a significantly higher variation relative to the expectation value. Where the average is about 1% 1100 nm have 1.6%.

Drift analysis

One tablet takes about 20 minutes to measure, all seven wavelengths. A significant drift during the measurement of one tablet would ruin our measurements. This is not the case as can be seen in Fig. 5.4. Measuring one full sample series of the 'API set' takes about 7 hours with breaks, once the cooling has stabilised.

Pressure used when making the tablets

There is an unwanted spread in pressure used when producing them. In order to understand the impact of this a set of 10 tablets were made using different pressure. The set was made at Astra Zeneca using an unsifted granulate 11.

From Fig. 5.5 it becomes clear that there is an increase in scattering for the tablets made with less than 2 tons of pressure. This trend is also visible in the thickness of these tablets and offer a likely physical explanation of this effect but whether this change in scattering is due to the increased thickness

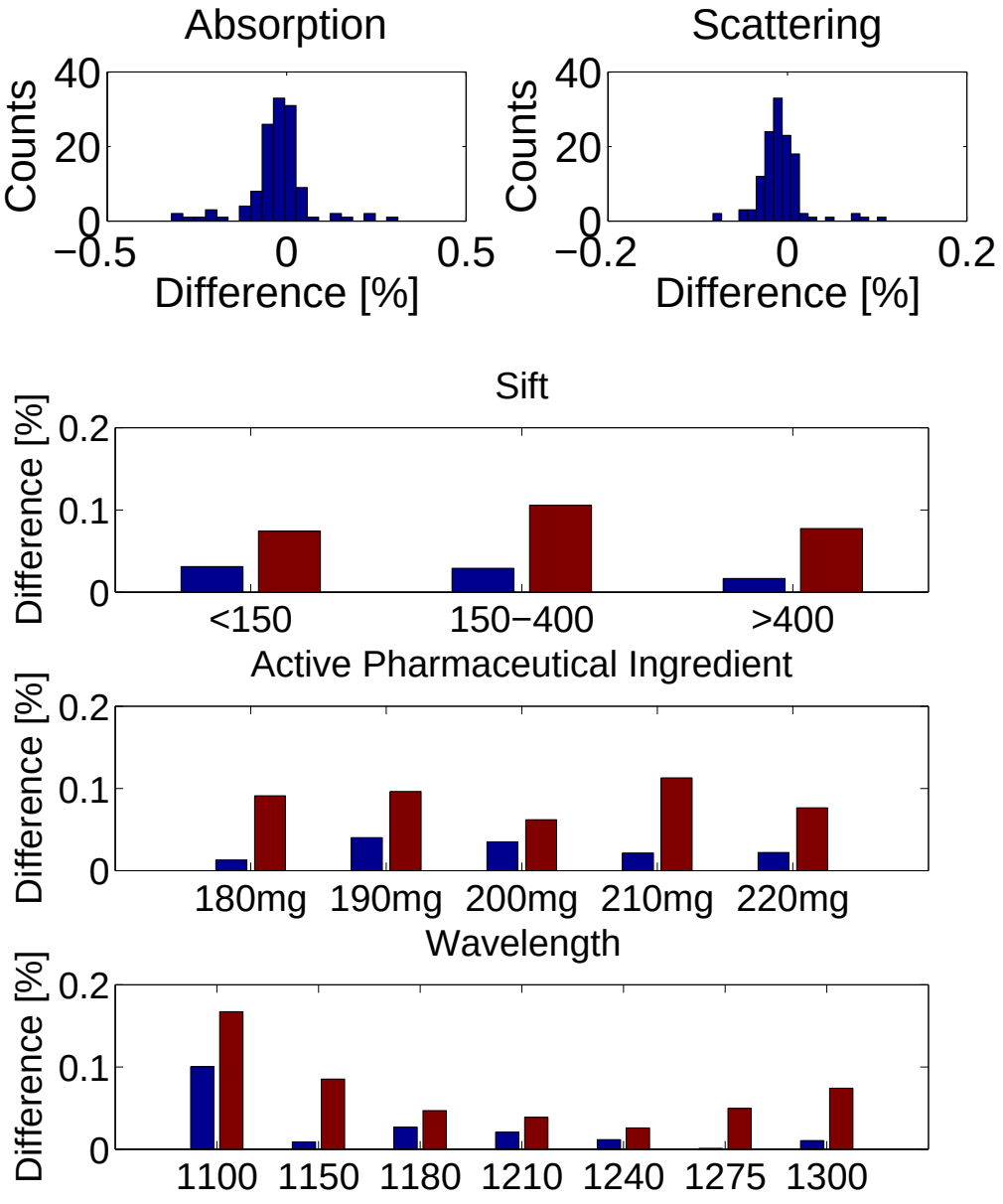

Figure 5.3: To the right, the difference in percent between a 'four measurement' and a 'long measurement'. To the left, the difference in absorption ordered in sift, API and wavelength. The blue bars are expectation values and the red bars are standard deviation.

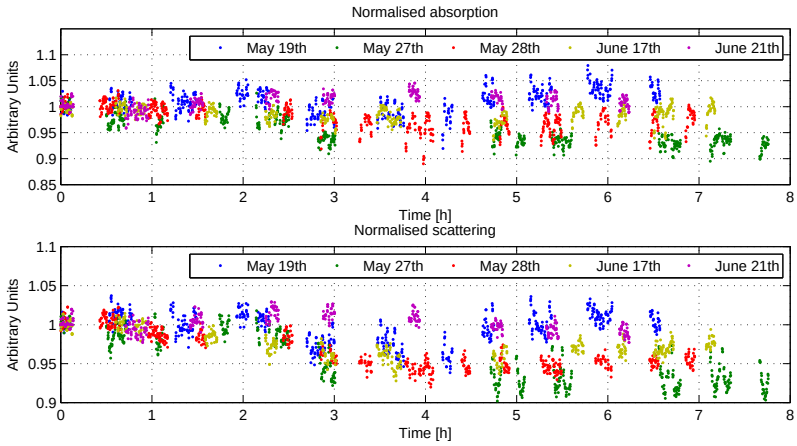

Figure 5.4: To measure the drift the first tablet measurement of the day is matched and analysed with every IRF measurement of the corresponding wavelength made the same day.

of the tablets, decreased density, deformation of the granulate particles or possibly an increased presence of air in the sample is to early to speculate in. There does not seem to be any significant change in the absorption as seen in Fig. 5.5. This is a very good sign as it shows that the decoupling between absorption and scattering is working to some degree.

Fiber width

The model used when fitting to measurement in order to calculate absorption and scattering is using a point source and a point detector. This could easily be solved using e.g. numeric integrating but it would radically increase the computation time. As seen in Fig. 5.6 fitting the point to point model to a model that uses numeric integration to simulate the width shows that the scattering is overestimated by almost 1% increasing slightly with increasing μ_s and and μ_a. The absorption error decrease when μ_a increase. This will not create any problem for our measurements as it does not affect the precision only the accuracy of our measurements.

Tablet width

Another problem of the diffusion approximation is that it assumes an infinite width contrary to the tablets 1.3 cm diameter. Fitting DA to MC simulations of tablets of 1 cm diameter done earlier by Erik Alerstam give both an increased absorption and scattering. Results are shown in Tab. 5.2.

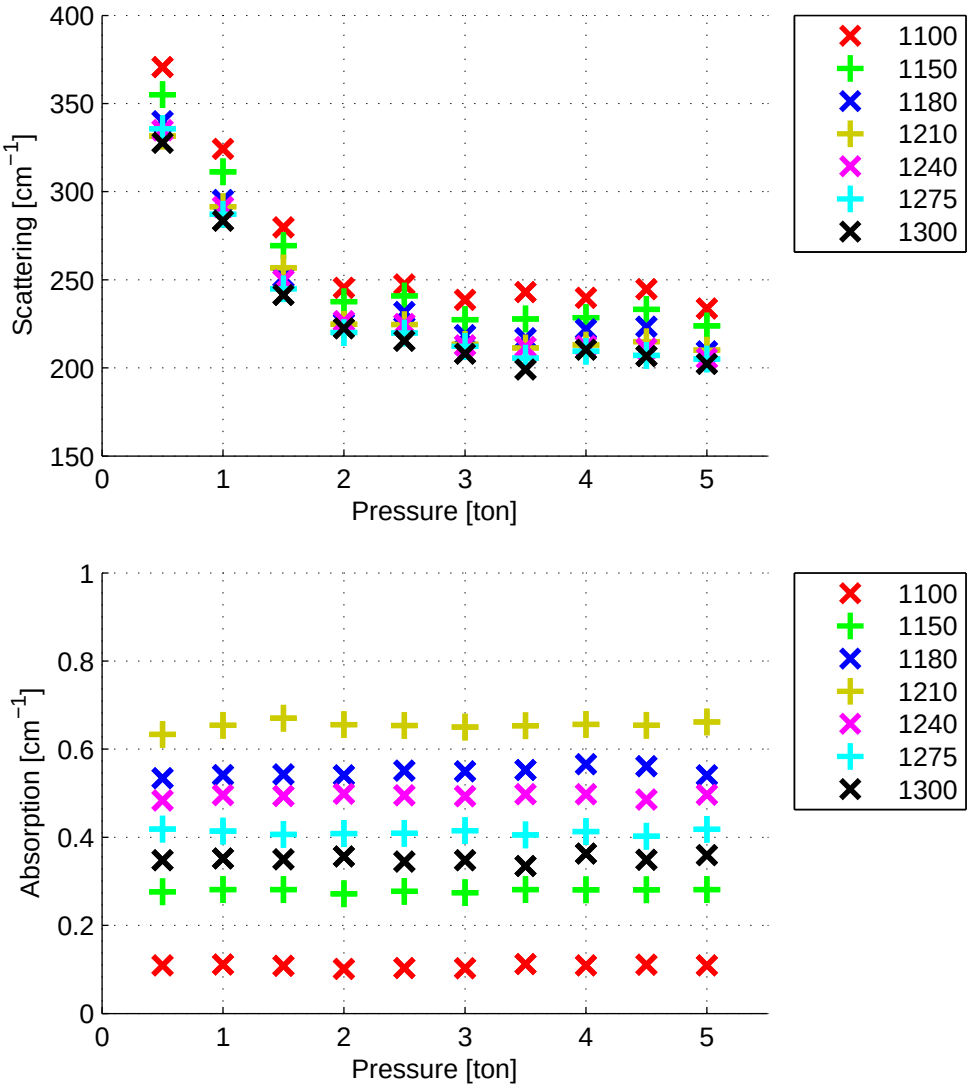

Figure 5.5: Absorption and scattering vs pressure for the 'pressure set'

Pressure [ton]	Thickness [mm]
<1	3.24
1	3.12
1.5	2.88
2	2.89
2.5	2.98
3	2.82
3.5	2.95
4	2.90
4.5	2.85
5	3.00

Table 5.1: This table show the thickness of the tablets in the 'pressure set' and how much pressure was used to make them. The thickness start increasing when less than 2 tons pressure is used. When more than 2 tons of pressure is used the tablet thickness seems to be pressure independent.

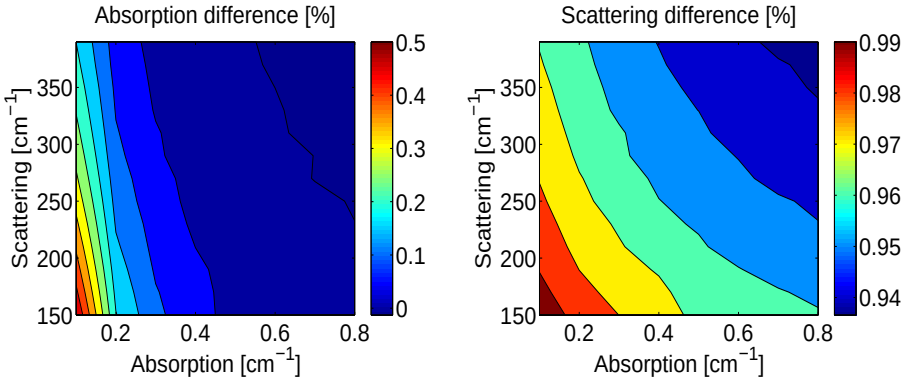

Figure 5.6: To the right, a graph of the overestimation of absorption in percent. To the left, a graph of the overestimation of scattering in percent.

		Absorption		
		0.3	0.5	0.7
Scattering	100	0.348 105	0.555 105	0.761 105
	400	0.307 401	0.556 421	0.791 429
	700	0.341 740	0.581 777	0.756 726

Table 5.2: The analysis of the MC simulations with limited tablet width for three different sets of scattering and absorption.

There is an increased variance with increasing scattering as more photons are needed to achieve the same variance for a higher scattering. Over all there is about a 5% increase in scattering and 10% increase in absorption.

5.3 Concentration measurements

The measured results of the 'API tablets sets' are shown separately according to their sift size, granulate and wavelength. The sift size graph, Fig. 5.9, shows how the scattering is affected by different physical properties such as particle size. The below 150 μm sift have a significantly higher scattering compared to the rest as it covers a bigger relative size span with respect to other sifts. This in line with Mie theory where particle size and shape is one of the major factors to scattering. This is also demonstrated in Fig. 5.8 where all 52 tablets span 150 cm^{-1} for the scattering but the absorption spread within a wavelength only span 0.1 cm^{-1}. The distinguishing features of the different granulates are hidden in the noise, Fig. 5.7. As we can see in the graph the two most different granulates are 17 and 19. These two granulates are supposedly chemically identical, except for the Metoprolol which are made in different batches.

5.4 PLS regression

To calculate the API concentration from the measured spectra we use PLS regression on the measurements, results seen in Fig. 5.11 and Fig. 5.10. Explained variance is how much the variance is reduced when a factor is taken into account. The variance is then improved by 20.5% when including the first PC in the evaluation. The baseline is just using the mean API concentration without regard for the absorption and it gives a mean squared

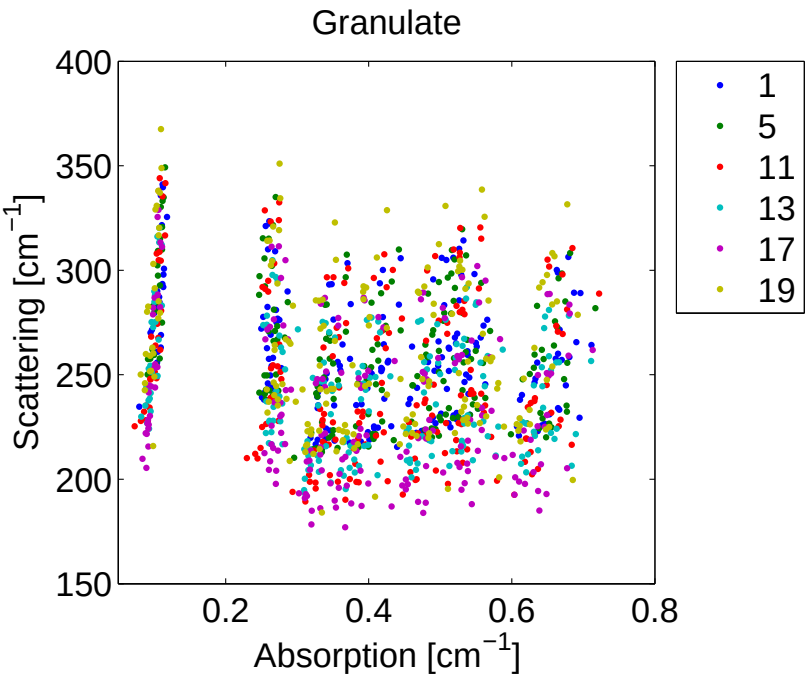

Figure 5.7: Absorption vs scattering for granulates at different wavelengths.

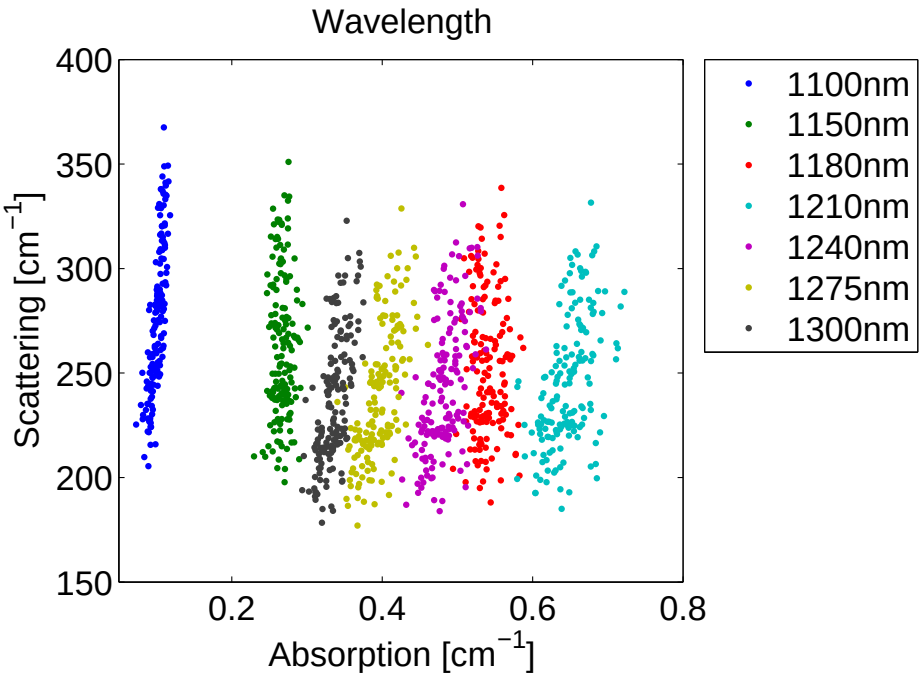

Figure 5.8: Absorption vs scattering for different wavelengths.

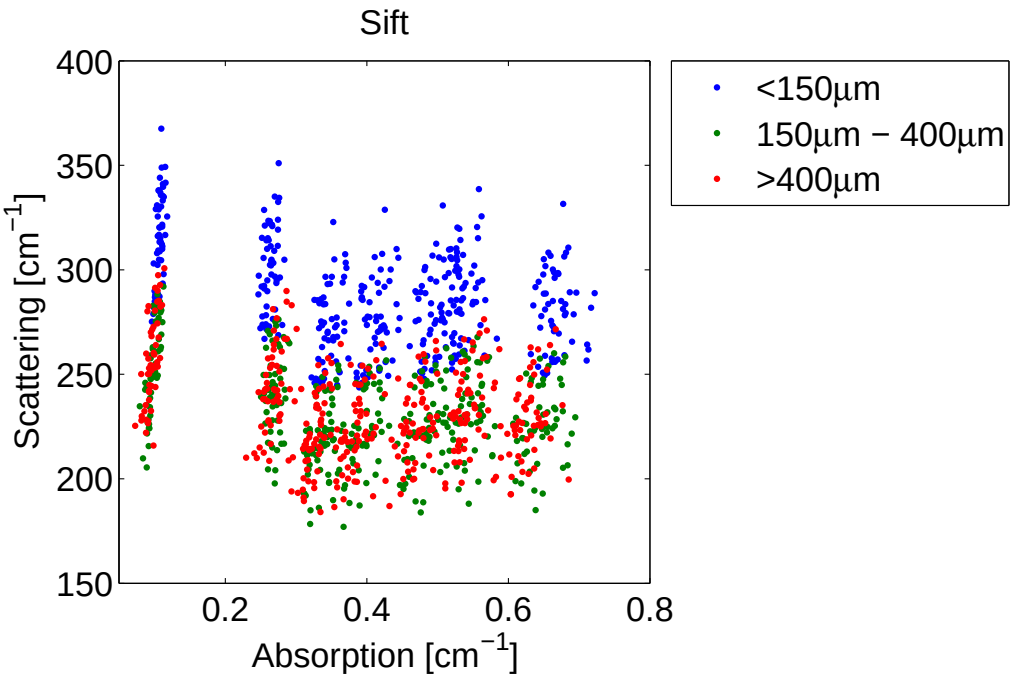

Figure 5.9: Absorption vs scattering for sifts at different wavelengths.

error, MSE, of 225. If we use PLS on individual sifts we explain much more of the variance, see table A.1 in the appendix.

From the explained variance in the table you can see that there really is no point to use more than 5 component as the result only get marginally better. There is also likely no reason to use more than 3 components as those beyond that are likely to be dominated by measurement noise. The estimated API concentrations can be seen in Fig. 5.11. From the result we can then estimate the API concentration within 15%.

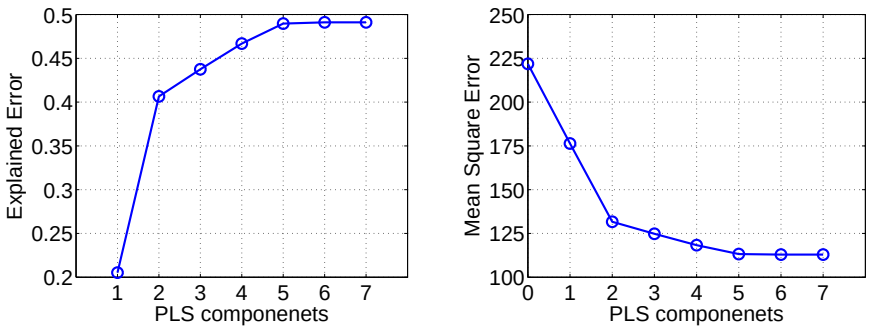

Figure 5.10: An evaluation of the PLS regression of our data. It contains the explained variance and mean squared error of the fitting of API concentrations for different number of PLS components. After 5 components there is very little need to use the rest.

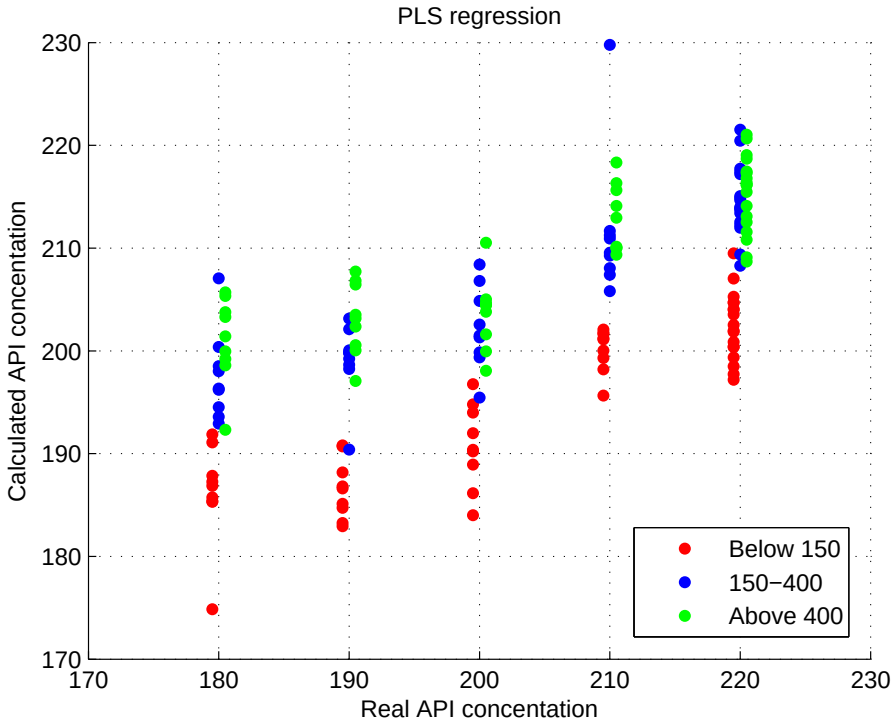

Figure 5.11: The estimated API concentrations using only 3 PLS components differentiating between sift size. The results have been shifted a little along the x-axis for convenience.

Chapter 6

Conclusion

We have measured all the 52 tablets at 7 different wavelengths, at least twice. The absorption and scattering are measured within 2.13% precision. After a PLS regression we can distinguish between the highest and lowest API concentration in our tablet set. We can predict the API concentration within 5% if the PLS regression is done on *only* one sift.

We still think it is possible to accurately measure the API concentration of the whole set so that all the API concentrations are separable. We still have ideas on what can be improved. If we had measured a reference tablet i.e. epoxy tablet, each day of measurements we could have used it to correct for the daily drifts. If the 'API set' would have had a wider API span, the PLS regression would have had a better signal-to-noise ratio. It would also be worth testing to use MC modelling to evaluate the time of flight distribution.

It is likely that some of the errors in our measurements would disappear with a stable cooling.

Chapter 7

Acknowledgements

Dmitry
Erik
Stefan
Jonas
Atomic Physics Department
Astra Zenica

Appendix A

Appendix

Separating the sifts

All the sifts

PLS components	0	1	2	3	4	5	6	7
Explained variance	—	0.205	0.407	0.438	0.467	0.490	0.491	0.491
Mean square error	225.0	180.2	137.3	143.3	132.5	127.1	124.7	125.0

Only the above 400μm sift

PLS components	0	1	2	3	4	5	6	7
Explained variance	—	0.313	0.700	0.801	0.815	0.820	0.821	0.821
Mean square error	230.7	167.0	78.02	54.26	54.14	55.47	56.02	56.15

Only the 400μm to 150μm sift

PLS components	0	1	2	3	4	5	6	7
Explained variance	—	0.391	0.776	0.820	0.845	0.848	0.848	0.848
Mean square error	229.7	145.5	58.05	52.09	45.72	46.68	46.97	46.88

Only the below 150μm sift

PLS components	0	1	2	3	4	5	6	7
Explained variance	—	0.253	0.740	0.785	0.797	0.803	0.806	0.806
Mean square error	230.7	189.2	109.3	157.2	132.6	114.4	147.0	171.7

Table A.1: An evaluation of four different PLS regressions of our data. It contains the explained variance and mean squared error of the fitting of API concentrations for different number of PLS components. After 5 components there is very little need to use the rest.

Bibliography

[1] Dimofte A, Finlay JC, Zhu TC
A method for determination of the absorption and scattering properties interstitially in turbid media
Phys Med Biol 50 2291-2311 (2005)

[2] R. Graaff, J. G. Aarnoudse, J. R. Zijp, P. M. A. Sloot, F. F. M. de Mul, J. Greve, and M. H. Koelink
"Reduced light-scattering properties for mixtures of spherical particles: a simple approximation derived from Mie calculations"
Appl. Opt. 31, 1370-1376 (1992)

[3] MacDonald B. F. et al.
Some Applications of Near-Infrared Reflectance Analysis in the harmaceutical Industry
Journal of Pharmaceutical and Biomedical Analysis; vol. 11, No. 11-12, 1993, pp. 1077-1085, XP001098341; ISSN: 0731-7085; p. 1079

[4] Colin N. Benwell and Elaine M. McCash
Fundamental of Molecular Spectroscopy
4th Edition. The MacGraw-Hill companies.

[5] Barbara H.Staurt
Infrared spectroscopy: fundamentals and applications
John Wiley and Sons, Ltd.

[6] Blanco, M., et al.
Identification and Quantitation Assays for Intact Tablets of Two Related Pharmaceutical Preparations by Reflectance Near-Infrared Spectroscopy: Validation of the Procedure
Journal of Pharmaceutical and Biomedical Analysis; vol. 22, No. 1, Feb.

2000, pp. 139-148

[7] Christoffer Abrahamsson, Jonas Johansson,, Stefan Andersson-Engels,, Sune Svanberg, and, Staffan Folestad
Time-Resolved NIR Spectroscopy for Quantitative Analysis of Intact Pharmaceutical Tablets
Analytical Chemistry 2005 77 (4), 1055-1059

[8] Ramirez JL, Bellamy MK, Romanach RJ.
A Novel Method for Analyzing Thick Tablets by Near Infrared Spectroscopy.
AAPS PharmSciTech. 2001; 2(3): article 11.

[9] M. Blanco, J. Coello, H. Iturriaga, S. Maspoch and N. Pou
Influence of the procedure used to prepare the calibration sample set on the performance of near infrared spectroscopy in quantitative pharmaceutical analyses
Analyst, 2001, 126, 1129-1134

[10] Daniele Contini, Fabrizio Martelli, and Giovanni Zaccanti,
Photon migration through a turbid slab described by a model based on diffusion approximation. I. Theory.
Applied Optics, Vol. 36, Issue 19, pp. 4587-4599 (1997)

[11] Henri Gavin
The Levenberg-Marquardt method for nonlinear least squares curve-fitting problems
http://www.duke.edu/ hpgavin/ce281/lm.pdf
Department of Civil and Environmental Engineering
Duke University
January 12, 2009

[12] L.Eriksson, E.Johansson, N.Kettaneh-wold and S.Wold
Introduction to Multi- and Mega-variate Data analysis techniques using projection methods.

[13] *Time correlated single photon counting modules - operating manual*
www.becker-hickle.de
2005

[14] A. Farina, A. Bassi, A. Pifferi, P. Taroni, D. Comelli, L. Spinelli, and R. Cubeddu
Bandpass Effects in Time-Resolved Diffuse Spectroscopy
Appl. Spectrosc. 63, 48-56 (2009)